

This document is the Accepted Manuscript version of a Published Work that appeared in final form in the Journal of Physical Chemistry Letter, copyright © American Chemical Society after peer review and technical editing by the publisher. To access the final edited and published work see: <https://pubs.acs.org/doi/abs/10.1021/acs.jpcllett.7b02742>.

Nanoscopic Approach to Quantification of Equilibrium and Rate Constants of Complex Formation at Single-Molecule Level

Xuzhu Zhang,[†] Evangelos Sisamakos,[‡] Krzysztof Sozanski,[†] and Robert Holyst^{*,†}

*[†]Department of Soft Condensed Matter, Institute of Physical Chemistry, Polish Academy of
Sciences, Warsaw, Poland*

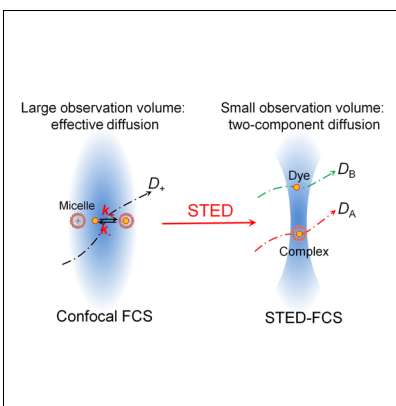
[‡]PicoQuant GmbH, Berlin, Germany

E-mail: rholyst@ichf.edu.pl

Abstract

Equilibrium and rate constants are key descriptors of complex-formation processes in a variety of chemical and biological reactions. However, these parameters are difficult to quantify, especially in the locally confined, heterogeneous, and dynamically changing living matter. Herein, we address this challenge by combining stimulated emission depletion (STED) nanoscopy with fluorescence correlation spectroscopy (FCS). STED reduces the length-scale of observation to tens of nanometres (2D)/attoliters (3D) and the time-scale – to microseconds, with direct, gradual control. This allows to distinguish diffusional and binding processes of complex-formation even at reaction rates higher by an order of magnitude than in confocal FCS. We provide analytical autocorrelation formulas for probes undergoing diffusion-reaction processes under STED condition. We support the theoretical analysis of experimental STED-FCS data on a model system of dye-micelle, where we retrieve the equilibrium and rates constants. Our work paves a promising way towards quantitative characterization of molecular interactions *in vivo*.

Graphical TOC Entry

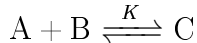


Although non-covalent interactions are generally much weaker than covalent bonding, they significantly affect the physicochemical properties of matters and play a crucial role in the processes of complex formation in biochemical and supramolecular systems.¹ Determination of equilibrium and rate constants of these interactions can provide quantitative information on these systems.^{2,3} Complex formation processes are often extremely fast (up to the diffusion-controlled limit) and require highly advanced techniques to study them quantitatively.⁴⁻⁷ The main methods used previously, e.g. NMR, titration, sometime gave relatively inconsistent results since individuals' behaviours of molecules were averaged in the experiments.^{3,8,9} Single-molecule techniques are ideal tools for the characterization of molecular interactions. One of the most promising experimental solutions is the fluorescence correlation spectroscopy (FCS).^{7,9-11} In FCS, fluctuations of fluorescence originating from probes diffusing through an observation volume are recorded. Autocorrelation of the signal reveals the characteristic time-scales of the fluctuations. Combined with a proper theoretical model, such analysis may offer various information on the physicochemical properties of the system,^{9,12} such as diffusion coefficients of the probes and dynamics of any reaction they are involved in. Due to the diffraction limit, the length-scale of observation volume in standard FCS experiments cannot be reduced below ~ 200 nm. However, this limitation can be circumvented by means of stimulated emission depletion (STED).

STED nanoscopy offers spatial resolution down to ~ 20 nm by employing a depleting laser beam (shaped into a "donut" with zero intensity at center) coaxial to the excitation beam.¹³⁻¹⁵ In principle, the depleting laser suppresses spontaneous fluorescence from the outer part of the confocal volume, trimming the effective observation volume to sub-diffraction size. Combination of STED with FCS (STED-FCS) allows to perform experiments at higher probe concentrations and shorter length-scales of observation volume than confocal FCS.¹⁶ This is particularly useful for biological¹⁷⁻¹⁹ and anomalous diffusion^{4,20} investigations. A number of such studies have been reported in 2D systems (e.g., lipid membranes).^{4,11,21,22} For instance, Eggeling et al revealed the single-molecular reaction dynamics

in the plasma membranes of live cells with STED-FCS.²³ The on/off rates of the binding of lipids to other membrane constituents were determined by the reaction-dominated model for the autocorrelation function. However, few studies using STED-FCS in solutions have been published. This is largely due to troublesome analysis and interpretation of STED-FCS data, related to non-3D-Gaussian observation volume and lack of the analytical form of autocorrelation function (ACF) for such systems.²⁴⁻²⁶ A recently proposed solution,²⁵ based on realistic description of the 3D observation volume under STED and empirically justified approximation of the ACF, allows to overcome these issues. Here, we develop this solution for quantitative studies of diffusion-reaction processes at sub-diffraction length-scales. A unique advantage of STED-FCS for binding/unbinding kinetics studies is direct, gradual control over the size of observation volume. This allows to cross in a single experimental system between the large "observation volume" regime, where multiple binding/unbinding acts occur while the probe resides in the observation volume and a single, effective diffusion coefficient is observed, and the "small observation volume" regime, where distinct populations of free and bound probe are observed.⁹⁻¹¹

In this Letter, we demonstrate a successful application of STED-FCS to quantification of the equilibrium and rate constants of supramolecular interactions on a simple model of fluorescent dye reversibly binding to surfactant micelles. The particular advantages of this model system have already been introduced previously:⁹ high stability of each component, simple interaction mechanism, no side-products, large difference in the diffusion coefficient between the free and bound probe, and full reversibility of the process. The molecular interaction between surfactant micelles (Octaethylene glycol monododecyl ether, C₁₂E₈ denoted by *A*) and the dye (ATTO647N, denoted by *B*) can be treated as a pseudo-first-order reaction:^{9,27}



where *C* stands for dye-micelle complexes. The equilibrium constant *K* is related to the association and dissociation rate constants (*k*₊, *k*₋) and the concentrations of each component at the equilibrium state (*[A]*^{eq}, *[B]*^{eq}, *[C]*^{eq}) as *K* = *k*₊/*k*₋ = *[C]*^{eq}/*[A]*^{eq}*[B]*^{eq}. The relaxation

rate R of the interaction, which describes the rate of the reaction returning to the equilibrium, is defined as $R = k_+([A]^{\text{eq}} + [B]^{\text{eq}}) + k_-$.²⁷ Because in the discussed experiments the micelle concentration is always much higher than the dye concentration, $[A] \gg [B] \approx 10^{-9}$ M, we introduce the following approximation:

$$R \approx k_+[A] + k_- = k_+[A] + k_+/K. \quad (1)$$

It follows that the higher the micelle concentration, the larger the relaxation rate of dye-micelle interaction (i.e., the shorter the time of the return to the equilibrium).

Depending on the ratio of the average time spent by the dye in the observation volume (determined by the volume size) and the relaxation rate, qualitatively different regimes can be distinguished in terms of autocorrelation data analysis. In the large volume regime, the effective residence time of probes is substantially longer than the relaxation time ($1/R$), namely $\tau_{\Delta} \gg 1/R$. Then, equilibrium is established within the observation volume while the probe is detected. A single, effective diffusion coefficient is obtained, including multiple association/dissociation acts, as well as diffusion of free dyes and dye-micelle complexes in the intervening periods. Contrarily, in the small volume regime, the residence times are shortened and equilibrium is not attained inside the observation volume. There is not enough time for association/dissociation acts to occur before the probe diffuses out of the observation volume (i.e., $\tau_{\Delta} \ll 1/R$). Hence, motions of dye-micelle complexes and free dyes (D_A and D_B) are recorded separately. In the regime where $\tau_{\Delta} \approx 1/R$, neither of the two simplifications is valid and the full autocorrelation model including diffusion of the two species as well as the reaction needs to be applied. With a system characterized by an appropriate relaxation rate, it is possible to observe the transition between the aforementioned regimes, simply by controlling the size of the observation volume using STED (see Fig. 1a).

To allow for quantitative STED-FCS analysis in solutions, we apply the recently developed methodology based on a realistic model of the non-3D-Gaussian observation volume

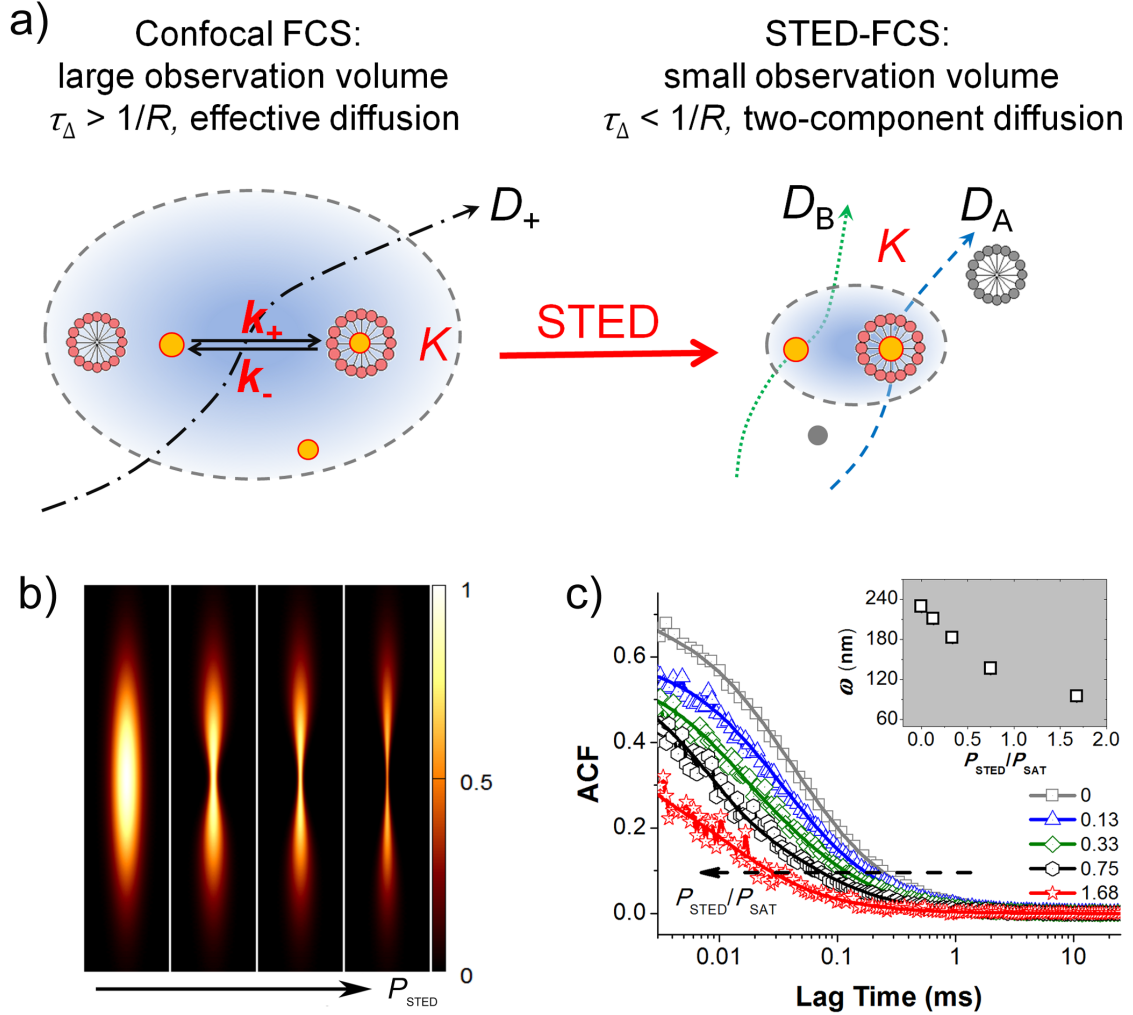


Figure 1: a) Schematic illustration of the complex formation processes in a dye-micelle system within a large and small observation volumes of STED-FCS. In the large volume, multiple association/dissociation acts occur during a single passage of the dyes through the observation volume and a single, effective diffusion coefficient is measured. In the small volume, diffusion overruns the reaction and two distinct components (free dyes and dye-micelle complexes) are observed. b) Representative profiles of effective observation volumes of STED-FCS under various STED powers P_{STED} . For details on the excitation, depletion, and observation profiles see section S3 in SI and Ref. 25. c) Experimental STED-FCS autocorrelation curves for ATTO647N diffusing in PBS (open symbols) under various values of $P_{\text{STED}}/P_{\text{SAT}}$ and the fits using Eq. 2 (solid lines). ATTO647N features high photostability and extremely low triplet state contribution to the ACF, so the triplet fraction is not included in the fitting processes. Insert: changes in the effective radii of the observation volume under various STED conditions determined from Eq. 3.

shape.²⁵ Briefly, the radial profile of a STED beam is given by a first-order Laguerre-Gaussian function.^{28,29} Its width evolves along the axial direction (see Fig. S2 in SI), causing most efficient depletion at the focal plane and relatively weaker influence on STED on the off-focus regions. This leads to the hourglass-like shape of the observation volume (see Fig. 1b and Fig. S2 in SI), as well as a decrease in the effective signal-to-noise ratio with increasing STED power due to high contribution of the fluorescence from the dim yet extensive fringes.²⁵ Still, each radial section of the observation volume retains a Gaussian profile. Due to strong elongation of the effective observation volume, the contribution of axial diffusion of the probes to the autocorrelation function is negligible. These factors justify application of a simple 2D autocorrelation fitting model, which for free dye diffusion is expressed as:

$$G_{2D}(\tau) = G(0)(1 + \tau/\tau_B)^{-1}, \quad (2)$$

where $G(0)$ is the ACF amplitude and τ_B is the residence time of the dye. This approximation has been validated by computer simulations and a series of experiments with different probes (radii ranging from 0.7 to 6.9 nm) and different medium compositions.²⁵

For free dyes diffusing in three dimension, τ_B appearing in Eq. 2 depends on its diffusion coefficient D_B and the radius of observation volume ω as:

$$\tau_B = \omega^2/4D_B. \quad (3)$$

Under STED conditions, ω in the focus plane decreases with STED power (P_{STED}) as:^{30,31} $\omega = \omega_0/\sqrt{1 + P_{\text{STED}}/P_{\text{SAT}}}$, where ω_0 is the radius of confocal observation volume. P_{SAT} is the saturation power, characteristic for a given fluorophore in given conditions, defined as the STED power at which the overall intensity of spontaneous fluorescence is decreased by half.^{13,31} However, the effective ω for STED-FCS in solution corresponds to the radius of the brightest sections of the observation volume and is not equivalent to the detection radius at the focal plane ($\omega(z = 0)$) due to the axial evolution of the STED profile.²⁵ Therefore, unlike

the experiments in 2D systems,^{4,21} ω for STED-FCS in solutions cannot be directly obtained from bead scanning experiments. Instead, a series of FCS measurements under various STED power settings for a reference probe with known diffusion coefficient need to be performed for the calibration of the dependence of effective ω on $P_{\text{STED}}/P_{\text{SAT}}$. The value of P_{SAT} of the reference probe was determined by finding the P_{STED} at which the fluorescence intensity dropped by half. In this work we used ATTO647N (with determined $P_{\text{SAT}} = 11$ mW, see Fig. S1 in SI) diffusing in phosphate-buffered saline (PBS), taking $D_{\text{B}} = 352 \mu\text{m}^2\text{s}^{-1}$ – this value was established in independent FCS measurements, performed at $T = 298$ K (see section S4 in SI).

As expected, experimental ACFs for ATTO647N in PBS shifted towards shorter lag time regions as the STED power increased. The diffusion times were obtained from the fits of the experimental curves using Eq. 2. Based on these values, we calculated ω according to Eq. 3. It decreased from 230 nm at zero STED to 95 nm at $P_{\text{STED}} \approx 1.7P_{\text{SAT}}$ (see the inset of Fig. 1c). Increasing the STED power even further led to ACFs of poor quality due to low signal-to-noise ratio (SNR) at high STED power.²⁵ In addition, there was no extra effects such as photobleaching of the dye, heating or optical trapping introduced by the low-power STED laser we employed in the experiments.³²

When we measured diffusion of ATTO647N in C_{12}E_8 solutions with FCS (at $P_{\text{STED}} = 0$), we observed gradual shifts of the autocorrelation curves towards the longer lag time region as the micelle concentration increased (Fig. 2). Since the viscosity experienced by ATTO647N in these relatively dilute solutions can be treated as constant and equal to the buffer viscosity,³³ we attributed the prolongation of the correlation time to the formation of dye-micelle complexes. All the autocorrelation function curves could be fitted with the simple 3D single-component model for FCS:⁹

$$G_{\infty}(\tau) = G(0)(1 + \tau/\tau_+)^{-1} \left(1 + \tau / (\kappa^2 \tau_+)\right)^{-1/2}, \quad (4)$$

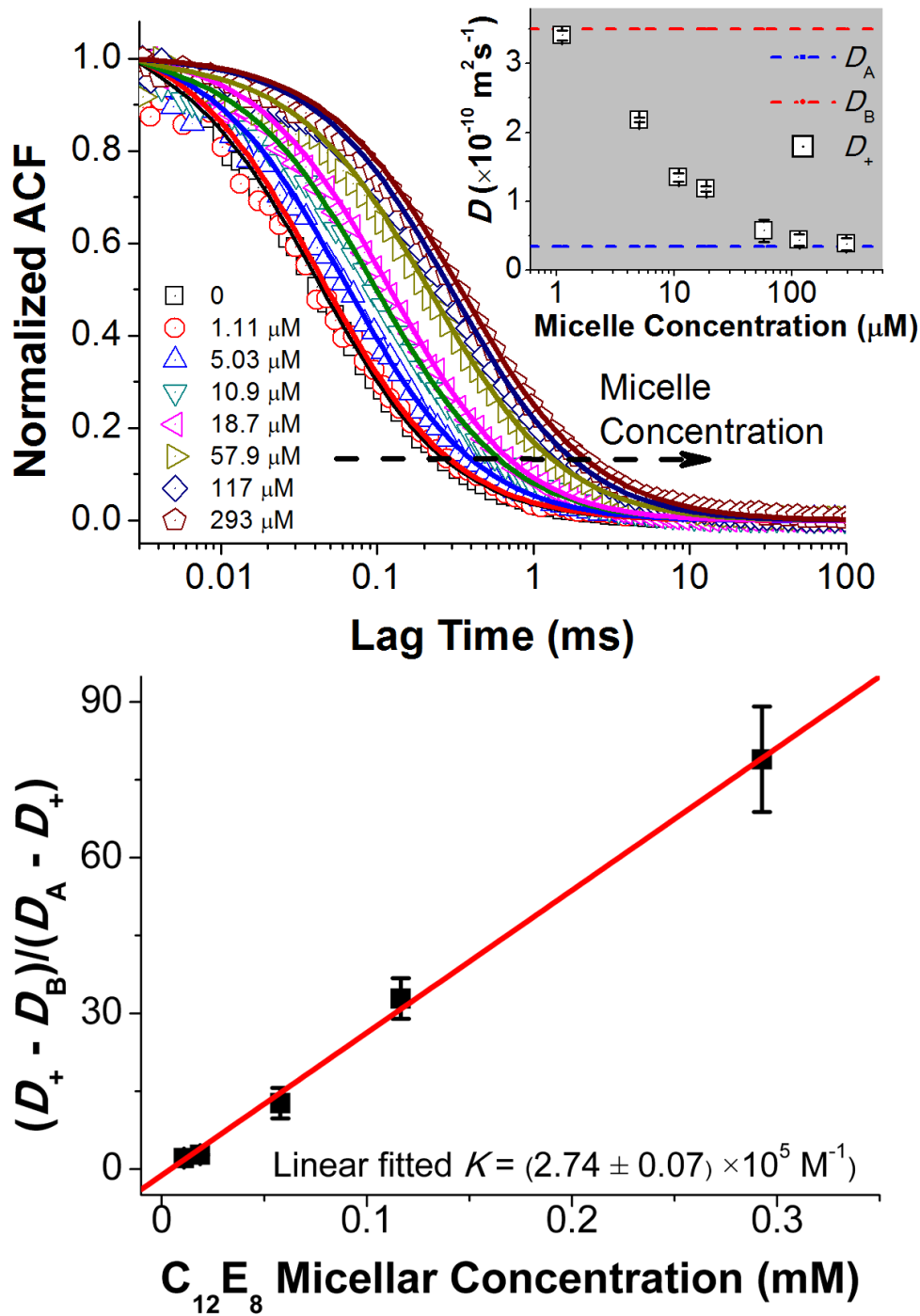


Figure 2: Upper panel: normalized experimental autocorrelation curves of ATTO647N in solutions of C_{12}E_8 of various concentrations (open symbols) and the fits (solid lines) using Eq. 4. Inset: measured diffusion coefficients of ATTO647N (red dash line, FCS measurements), C_{12}E_8 micelles (blue dash line, dynamic light scattering)⁹ and effective diffusion coefficients (D_+ , open rectangles) of ATTO647N in C_{12}E_8 solutions. Lower panel: equilibrium constant for ATTO647N/ C_{12}E_8 complex formation determined from the slope of the linear fitting using Eq. 5.

where structure parameter κ is the ratio of the long and short radii of the observation volume ellipsoid, equal to 6-8 in our fitting. Since this case fell within the large volume regime ($\tau_{\Delta} \gg 1/R$), multiple attachment/disattachment acts between the dye and micelles occurred during the probe's residence in the observation volume and averaged out to produce a single, effective value of diffusion time (τ_+). On this basis the effective diffusion coefficient, D_+ , was calculated using Eq. 3. In the low $C_{12}E_8$ concentration limit, D_+ approached the value characteristic for the dye diffusion in pure buffer. With increasing micelle concentration, D_+ gradually approached the value measured for self-diffusion of $C_{12}E_8$ micelles using dynamic light scattering ($0.34 \times 10^{-10} \text{m}^2\text{s}^{-1}$)⁹ – see the inset of Fig. 2. This proves the formation of dye-micelle complexes in the solutions and shows that at high micelle concentrations the dye spends most of the time as a part of the complex (and, after detachment, rapidly encounters another binding partner).

The equilibrium constant for the ATTO647N/ $C_{12}E_8$ complex formation was established from the slope of the linear dependence of D_+ on the concentration of micelles $[A]$ (see lower panel of Fig. 2), according to our previous work:⁹

$$K[A] = \frac{D_+ - D_B}{D_A - D_+} \quad (5)$$

The obtained value of $K = 2.74 \times 10^5 \text{M}^{-1}$ indicated a relatively stronger interaction than the case of $C_{12}E_8$ and rhodamine 110, described in our previous study.⁹ This probably resulted from the positive charge of ATTO647N that promoted its electrostatic attraction to the micelle shell.

For comparison, we also tried to fit the experimental autocorrelation curves with the two-component model, which would include contributions of the free dye and dye-micelle complexes separately. The diffusion times of both components were fixed on the basis of calibration data. However, the fits were of poor quality, revealing systematic deviations (see Fig. S4 in SI). This supported the claim that the equilibrium was established within the FCS

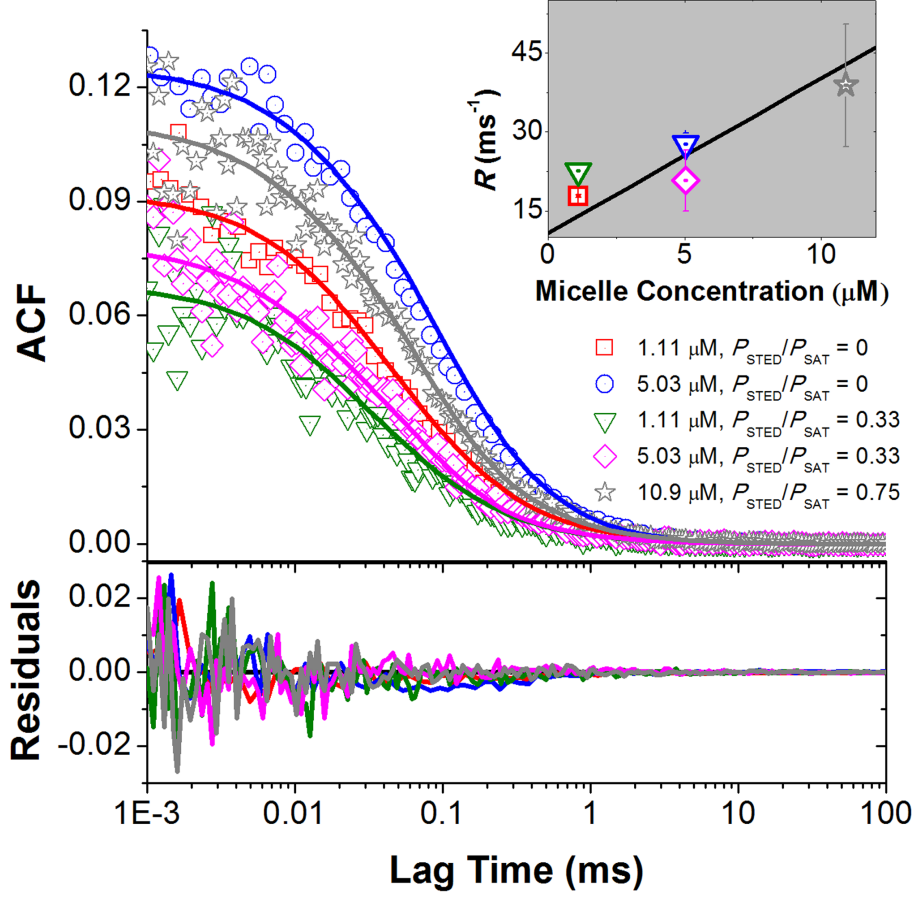


Figure 3: Experimental autocorrelation curves of ATTO647N in $C_{12}E_8$ solutions (1.11 – 10.9 μM , open symbols) under moderate STED conditions ($P_{\text{STED}}/P_{\text{SAT}} = 0 - 0.75$). The curves were fitted using the reaction-diffusion model of autocorrelation function (Eq. 6, solid lines) to obtain the chemical relaxation rates R of the reaction process, plotted as a function of micelle concentration in the inset. The association rate constant $k_+ = 2.95 \times 10^9 \text{ M}^{-1}\text{s}^{-1}$ was obtained from the slope of the fit according to Eq. 1 (black line), where K was fixed at the value determined from Eq. 5.

observation volume in this case, only permitting to observe the effective diffusion rather than the individual contributions of the substrate and the product.

To reach the intermediate range, where $\tau_{\Delta} \approx 1/R$, we performed experiments at moderate STED power ($P_{\text{STED}}/P_{\text{SAT}} = 0 - 0.75$) and low micelle concentrations (1.11 – 10.9 μM). Autocorrelation curves were fitted using the full model for the reaction-diffusion processes derived on the basis of Magde’s theory²⁷ and our previous work.^{9,10} The model is expressed

as:

$$\begin{aligned}
G_a(\tau) = G(0) & \left\{ (1 + \tau_+)^{-1} (1 + \tau / (\kappa^2 \tau_+))^{-1/2} \left[1 - \exp \left(-R\tau_\Delta \left(1 + \frac{\tau}{\tau_+} \right) \right) \right] \right. \\
& + \beta (1 + \tau_A)^{-1} (1 + \tau / (\kappa^2 \tau_A))^{-1/2} \exp \left(-R\tau_\Delta \left(1 + \frac{\tau}{\tau_+} \right) \right) + \\
& \left. (1 - \beta) (1 + \tau_B)^{-1} (1 + \tau / (\kappa^2 \tau_B))^{-1/2} \exp(-R\tau) \exp \left(-R\tau_\Delta \left(1 + \frac{\tau}{\tau_-} \right) \right) \right\}, \tag{6}
\end{aligned}$$

where $\tau_\pm = \omega^2/4D_\pm$, $\tau_\Delta = \omega^2/4D_\Delta$, $\tau_A = \omega^2/4D_A$, $\tau_B = \omega^2/4D_B$ are effective diffusion time of probes within the observation volume. The corresponding effective diffusion coefficients $D_+ = D_A\beta + D_B(1 - \beta)$, $D_- = D_A(1 - \beta) + D_B\beta$, $\Delta = D_A - D_B$, where $\beta = k_+[A]^{\text{eq}}/R = K[A]^{\text{eq}}/(1 + K[A]^{\text{eq}})$. The model features only one free parameter (R) which needs to be fitted, while the rest of the parameters (τ_\pm , τ_Δ , and β), whose values depend on the radius of observation volume, equilibrium constant and the micelle concentration, can be exactly fixed during the fitting procedure (e.g., K was fixed at the value determined from Eq. 5 on the basis of non-STED experiments). At the lowest concentration of micelles (1.11 μM) we obtained the minimum $R = 17.8 \text{ ms}^{-1}$, implying that the average time scale of the association/disassociation process (0.056 ms) was already much shorter than the diffusion time of dye-micelle complexes through the non-STED observation volume (0.39 ms) but slower than that of free dyes (0.038 ms). As expected, the relaxation rate of the dye-micelle interaction increased with the micelle concentration: the average distance between the dye and a micelle was shorter so that the diffusive search for another binding partner after detachment from the former one took less time. This led us back to the $\tau_\Delta \gg 1/R$ regime, where the reaction-diffusion model reached its limiting case of single-component model (cf. Eq. 4, and details see section S2 in SI). Then, only a single, effective diffusion coefficient was observed, which revealed no kinetic information. To keep the full reaction-diffusion autocorrelation model valid at higher micelle concentrations (i.e., to retain the $\tau_\Delta \approx 1/R$ condition), we reduced the diffusion times by means of cropping the observation volume using STED. All the values of R obtained from valid ACF fits using the full reaction-diffusion model

were plotted in the insert of Fig. 3 as a function of micelle concentration. The association rate constant ($k_+ = 2.95 \pm 0.32 \times 10^9 \text{ M}^{-1}\text{s}^{-1}$) was obtained from the slope of the linear fit using Eq. 1.

The retrieved k_+ value was roughly one order of magnitude smaller than the theoretical diffusion-limited value $k_{\text{dc}} = 2.29 \times 10^{10} \text{ M}^{-1}\text{s}^{-1}$. k_{dc} was estimated from the Smoluchowski equation: $k_{\text{dc}} = 4\pi D_{\text{AB}} R_{\text{AB}} N_{\text{A}}$, where N_{A} was the Avogadro constant, while D_{AB} and R_{AB} were, respectively, the sums of the diffusion coefficients and the hydrodynamic radii of the dye and the micelle. The difference between k_+ and k_{dc} stems from the mechanism of the dye-micelle complex formation. The micelle functions as a "soft cage" that hinders both entrance and exit of the dye molecule. We propose a simple two-step approximation to describe the dye-micelle interaction: (1) diffusion-controlled formation of $[A \bullet B]$ intermediate, described by the k_{dc} rate; (2) complex $[C]$ formation, realized by (at least partial) internalization of the dye into the micelle, driven by hydrophobic and electrostatic interactions. Stage (2) is the rate-determining step, with a rate was smaller than k_{dc} .⁹

Stability of the complex is inversely proportional to the disassociation rate constant k_- .³⁴ k_- can be calculated from the ratio of K to k_+ and for the ATTO647N/ C_{12}E_8 system equals $1.08 \pm 0.12 \times 10^4 \text{ s}^{-1}$. The equilibrium and rate constants for ATTO647N/ C_{12}E_8 determined from our experiments and model are close to the values reported for coumarine 152 and TX100 micelles by Bordello *et al.*³⁵

Further increase in the STED power in the dye-micelle systems and corresponding decrease in the diffusion times allowed us to reach the "small volume" regime, where $\tau_{\Delta} \ll 1/R$. This corresponds to the other limiting case of the autocorrelation model for reaction-diffusion, where diffusion times of all reagents are short enough to be observed irrespective of the attachment/disattachment events – at the time-scale of observation, the reaction can be treated as frozen. Knowing the disassociation rate k_- from the experiments in the reaction-diffusion regime, we estimated the lifetime of the complexes to be $\sim 0.1 \text{ ms}$.³⁴ Taking advantage of STED, we could decrease the diffusion time of the dye-micelle complexes below this critical

time-scale.

Therefore, at higher STED power ($P_{\text{STED}}/P_{\text{SAT}} > 0.75$) the appropriate model for ACF analysis is the simple two-component model:

$$G_0(\tau) = G(0) [\beta(1 + \tau/\tau_A)^{-1} + (1 - \beta)(1 + \tau/\tau_B)^{-1}], \quad (7)$$

where β is the fraction of complexes. Other parameters, such as the diffusion times of complexes (τ_A) and free dyes (τ_B) under STED condition can be calculated by Eq. 3 on the basis of calibration results. Results for ATTO647N diffusion in low-concentration micelle solutions at $P_{\text{STED}}/P_{\text{SAT}} = 1.7$ are presented in Fig. 4. The two-component model (with β as the sole fitting parameter, τ_A and τ_B as fixed parameters) provided high quality fits, with no systematic deviations. As expected, the fraction of dye-micelle complexes (β) increased with the micelle concentration. The equilibrium constant $K = 2.14 \times 10^5 \text{ M}^{-1}$, was determined on this basis as:

$$K[A] = \frac{\beta}{1 - \beta}. \quad (8)$$

This value is closely comparable to the value determined from the single-component model analysis of the non-STED experiments ($2.74 \times 10^5 \text{ M}^{-1}$).

Overall, we demonstrated the utility of STED-FCS for quantitative determination of equilibrium and rate constants of supramolecular interaction in solution. We provided a full analytical model for the autocorrelation function in a reaction-diffusion system upon STED conditions. Altering the size of observation volume, we were able to observe both limiting cases of the model: where a single, effective diffusion time is observed (equilibrium establishes within the time-scale of observation), and where separate contributions of free and bound dyes were observed (reaction slower than the time-scale of observation). The values of equilibrium constant determined for the ATTO647N/ $C_{12}E_8$ system in the two limiting cases were in reasonable agreement with each other. The association/dissociation rate constants were obtained from analysis of the experiments in the $\tau_{\Delta} \approx 1/R$ regime based on the full

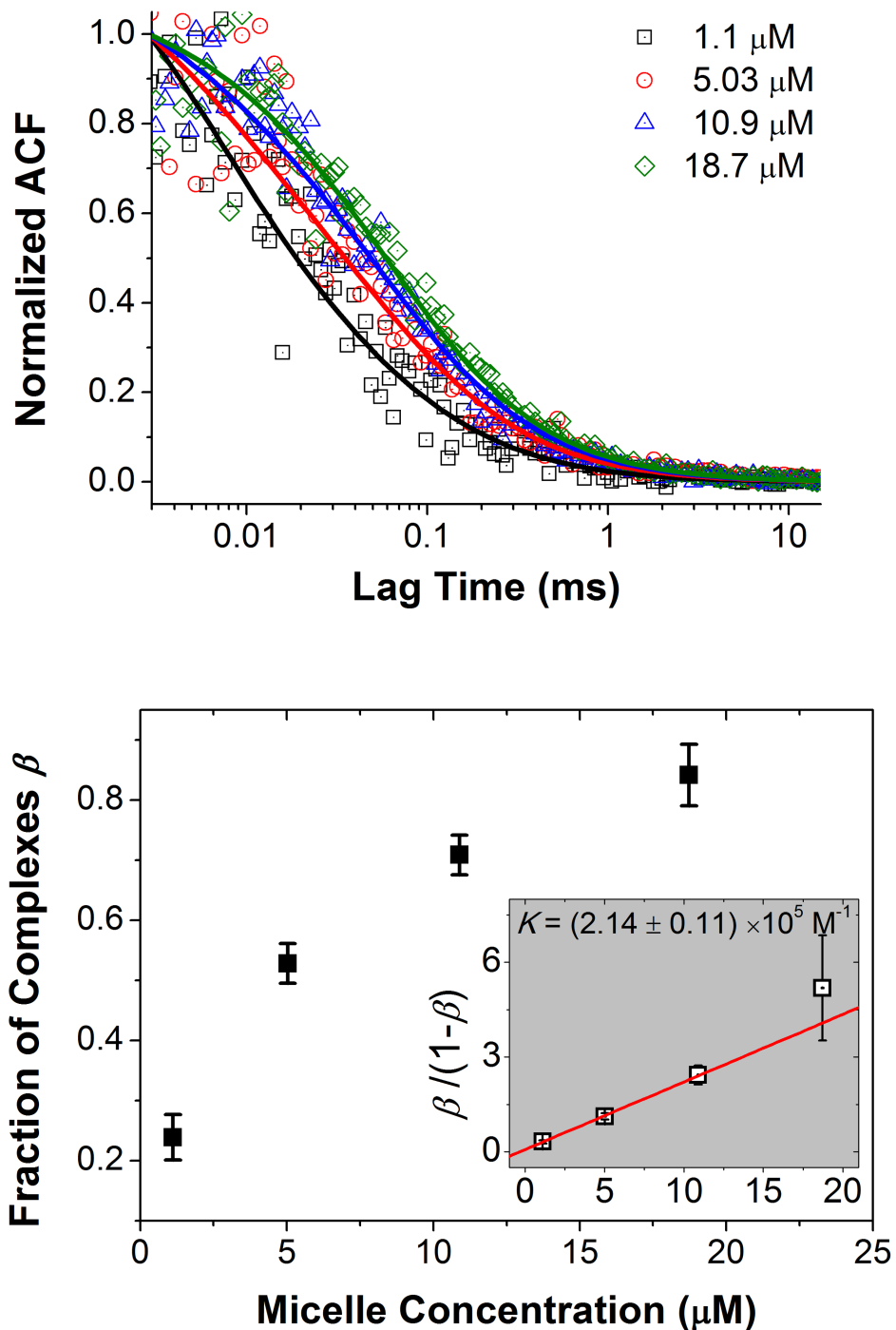


Figure 4: Upper panel: Normalized experimental (open symbols) and the fitting curves (solid lines) of ATTO647N diffusing in low concentrated C_{12}E_8 solutions under high STED power ($P_{\text{STED}}/P_{\text{SAT}} = 1.68$). The two-component model gave good fits to the experimental curves apparently. Lower panel: fractions of the dye-micelle complexes determined from the two-component model. Insert: equilibrium constant obtained from the slope of the linear fit using Eq. 8.

ACF model for reaction-diffusion. By demonstrating the applicability of STED to enhance the capabilities of FCS in kinetic studies, we showed a promising perspective for experimental realization of molecular interactions in simple solutions as well as biomimetic and biological complex systems.

Experimental Section

ATTO647N was purchased from AttoTec GmbH (Siegen, Germany). Surfactant C₁₂E₈ (purity: 99%) was purchased from Fluka. All chemicals were used without further purification.

STED-FCS experiments were conducted with MicroTime 200 (PicoQuant, Berlin, Germany) time-resolved fluorescence microscope with a STED add-on and a 100×/1.4 oil immersion objective (Olympus M Plan Aplanachromat). The system was equipped with the *easy*STED phase plate set³⁶ to form a depletion beam in donut-shape where the intensity of the depleting beam at the center was around 1% of its maximum, while the excitation beam was unaffected. Excitation and depletion lasers (LDH-640 and VisIR 765, PicoQuant)³⁷ were operated in pulsed mode. To increase the data quality and resolution of STED-FCS, long accumulation time of measurements (2-4 minutes) and time-gated approach was applied^{32,38-40} (for details see section S1 in SI). The frequency of the STED laser was set to 1/2 of the excitation laser, and therefore an intrinsic, synchronized non-STED reference was recorded in each measurement (cf. Fig. S1).⁴¹ So in one measurement we acquired data in both "confocal" and "confocal+STED" modality, without the need for extra series of measurements. This allowed to use the ratio of diffusion times of the probes under STED condition to the ones under confocal modality ($\tau_{\text{STED}}/\tau_{\text{confocal}}$) to describe the changes in the apparent probe behavior with the length-scale of observation, rather than the absolute τ_{STED} values – therefore, any errors related to the non-perfect shape of the beam were largely eliminated. Measurements were done in 8-well Lab-Tek chambered coverglass. Additional CCD camera was equipped in the system for detecting the light reflected from the sample

surface. This allows for highly reproducible and accurate positioning of the observation volume just above the coverglass, minimizing the aberrations related to the refractive index mismatch. Data analysis was performed in SymPhoTime x64 and Gnuplot (version 4.5). Further experimental details can be found in section S1 of SI.

Acknowledgement

The work was supported by the National Science Centre, Poland within the grant Maestro UMO-2016/22/A/ST4/00017. Part of this work was inspired by ERA CHAIR grant No 666295 from European Union's Horizon 2020 research and innovation programme.

Supporting Information Available

The Supporting Information is available free of charge on the website: Additional experimental details, short derivation of the full reaction-diffusion model for autocorrelation function and discussion on its limiting cases and application scopes, details on the 3D depletion and detection profiles of STED-FCS, determination of the diffusion coefficient of ATTO647N.

References

- (1) Anslyn, E. V.; Dougherty, D. A. *Modern Physical Organic Chemistry*; University Science Books, 2006.
- (2) Zheng, X.; Li, Z.; Podariu, M. I.; Hage, D. S. Determination of rate constants and equilibrium constants for solution-phase drug-protein interactions by ultrafast affinity extraction. *Anal. Chem.* **2014**, *86*, 6454–6460.
- (3) Thordarson, P. Determining association constants from titration experiments in supramolecular chemistry. *Chem. Soc. Rev.* **2011**, *40*, 1305–1323.

- (4) Eggeling, C.; Ringemann, C.; Medda, R.; Schwarzmann, G.; Sandhoff, K.; Polyakova, S.; Belov, V. N.; Hein, B.; von Middendorff, C.; Schönle, A. et al. Direct observation of the nanoscale dynamics of membrane lipids in a living cell. *Nature* **2009**, *457*, 1159–1162.
- (5) Bielejewska, A.; Bylina, A.; Duszczyk, K.; Fiałkowski, M.; Hołyst, R. Evaluation of ligand-selector interaction from effective diffusion coefficient. *Anal. Chem.* **2010**, *82*, 5463–5469.
- (6) Majcher, A.; Lewandowska, A.; Herold, F.; Stefanowicz, J.; Słowiński, T.; Mazurek, A. P.; Wieczorek, S. A.; Hołyst, R. A method for rapid screening of interactions of pharmacologically active compounds with albumin. *Anal. Chim. Acta* **2015**, *855*, 51–59.
- (7) Al-Soufi, W.; Reija, B.; Novo, M.; Felekyan, S.; Kühnemuth, R.; Seidel, C. A. Fluorescence correlation spectroscopy, a tool to investigate supramolecular dynamics: inclusion complexes of pyronines with cyclodextrin. *J. Am. Chem. Soc.* **2005**, *127*, 8775–8784.
- (8) Bujalowski, W. Thermodynamic and kinetic methods of analyses of protein- nucleic acid interactions. From Simpler to More Complex Systems. *Chem. Rev.* **2006**, *106*, 556–606.
- (9) Zhang, X.; Poniewierski, A.; Jelińska, A.; Zagożdżon, A.; Wisniewska, A.; Hou, S.; Hołyst, R. Determination of equilibrium and rate constants for complex formation by fluorescence correlation spectroscopy supplemented by dynamic light scattering and Taylor dispersion analysis. *Soft Matter* **2016**, *12*, 8186–8194.
- (10) Hołyst, R.; Poniewierski, A.; Zhang, X. Analytical form of the autocorrelation function for the fluorescence correlation spectroscopy. *Soft Matter* **2017**, *13*, 1267–1275.
- (11) Michelman-Ribeiro, A.; Mazza, D.; Rosales, T.; Stasevich, T. J.; Boukari, H.; Rishi, V.; Vinson, C.; Knutson, J. R.; McNally, J. G. Direct measurement of association and

- dissociation rates of DNA binding in live cells by fluorescence correlation spectroscopy. *Biophys. J.* **2009**, *97*, 337–346.
- (12) Zhang, X.; Poniewierski, A.; Hou, S.; Sozański, K.; Wisniewska, A.; Wieczorek, S. A.; Kalwarczyk, T.; Sun, L.; Hołyst, R. Tracking structural transitions of bovine serum albumin in surfactant solutions by fluorescence correlation spectroscopy and fluorescence lifetime analysis. *Soft matter* **2015**, *11*, 2512–2518.
- (13) Westphal, V.; Hell, S. W. Nanoscale resolution in the focal plane of an optical microscope. *Phys. Rev. Lett.* **2005**, *94*, 143903.
- (14) Hell, S. W.; Wichmann, J. Breaking the diffraction resolution limit by stimulated emission: stimulated-emission-depletion fluorescence microscopy. *Opt. Lett.* **1994**, *19*, 780–782.
- (15) Klar, T. A.; Hell, S. W. Subdiffraction resolution in far-field fluorescence microscopy. *Opt. Lett.* **1999**, *24*, 954–956.
- (16) Kastrup, L.; Blom, H.; Eggeling, C.; Hell, S. W. Fluorescence fluctuation spectroscopy in subdiffraction focal volumes. *Phys. Rev. Lett.* **2005**, *94*, 178104.
- (17) Huang, B.; Babcock, H.; Zhuang, X. Breaking the diffraction barrier: super-resolution imaging of cells. *Cell* **2010**, *143*, 1047–1058.
- (18) Müller, T.; Schumann, C.; Kraegeloh, A. STED microscopy and its applications: new insights into cellular processes on the nanoscale. *ChemPhysChem* **2012**, *13*, 1986–2000.
- (19) Niehorster, T.; Loschberger, A.; Gregor, I.; Kramer, B.; Rahn, H.-J.; Patting, M.; Koberling, F.; Enderlein, J.; Sauer, M. Multi-target spectrally resolved fluorescence lifetime imaging microscopy. *Nat. Methods* **2016**, *13*, 257–262.
- (20) Banks, D. S.; Tressler, C.; Peters, R. D.; Hoffing, F.; Fradin, C. Characterizing anomalous diffusion in crowded polymer solutions and gels over five decades in time with

- variable-lengthscale fluorescence correlation spectroscopy. *Soft Matter* **2016**, *12*, 4190–4203.
- (21) Mueller, V.; Honigmann, A.; Ringemann, C.; Medda, R.; Schwarzmann, G.; Eggeling, C. FCS in STED microscopy: studying the nanoscale of lipid membrane dynamics. *Methods Enzymol.* **2013**, *519*, 1–38.
- (22) Vicidomini, G.; Ta, H.; Honigmann, A.; Mueller, V.; Clausen, M. P.; Waithe, D.; Galiani, S.; Sezgin, E.; Diaspro, A.; Hell, S. W. et al. STED-FLCS: an advanced tool to reveal spatiotemporal heterogeneity of molecular membrane dynamics. *Nano Lett.* **2015**, *15*, 5912–5918.
- (23) Ringemann, C.; Harke, B.; Von Middendorff, C.; Medda, R.; Honigmann, A.; Wagner, R.; Leutenegger, M.; Schönle, A.; Hell, S. W.; Eggeling, C. Exploring single-molecule dynamics with fluorescence nanoscopy. *New J. Phys.* **2009**, *11*, 103054.
- (24) Lanzaò, L.; Scipioni, L.; Di Bona, M.; Bianchini, P.; Bizzarri, R.; Cardarelli, F.; Diaspro, A.; Vicidomini, G. Measurement of nanoscale three-dimensional diffusion in the interior of living cells by STED-FCS. *Nat. Commun.* *8*, 26417–26429.
- (25) Sozanski, K.; Sisamakias, E.; Zhang, X.; Holyst, R. Quantitative Fluorescence Correlation Spectroscopy in 3D Systems under Stimulated Emission Depletion Conditions. *Optica* **2017**, *4*, 982–988.
- (26) King, J. T.; Yu, C.; Wilson, W. L.; Granick, S. Super-resolution study of polymer mobility fluctuations near c . *ACS nano* **2014**, *8*, 8802–8809.
- (27) Magde, D.; Elson, E. L.; Webb, W. W. Fluorescence correlation spectroscopy. II. An experimental realization. *Biopolymers* **1974**, *13*, 29–61.
- (28) Török, P.; Munro, P. The use of Gauss-Laguerre vector beams in STED microscopy. *Opt. Express* **2004**, *12*, 3605–3617.

- (29) Tressler, C.; Stolle, M.; Fradin, C. Fluorescence correlation spectroscopy with a doughnut-shaped excitation profile as a characterization tool in STED microscopy. *Opt. Express* **2014**, *22*, 31154–31166.
- (30) Leutenegger, M.; Eggeling, C.; Hell, S. W. Analytical description of STED microscopy performance. *Opt. Express* **2010**, *18*, 26417–26429.
- (31) Harke, B.; Keller, J.; Ullal, C. K.; Westphal, V.; Schönle, A.; Hell, S. W. Resolution scaling in STED microscopy. *Opt. Express* **2008**, *16*, 4154–4162.
- (32) Clausen, M. P.; Sezgin, E.; de la Serna, J. B.; Waithe, D.; Lagerholm, B. C.; Eggeling, C. A straightforward approach for gated STED-FCS to investigate lipid membrane dynamics. *Methods* **2015**, *88*, 67–75.
- (33) Kalwarczyk, T.; Ziebach, N.; Bielejewska, A.; Zaboklicka, E.; Koynov, K.; Szymanski, J.; Wilk, A.; Patkowski, A.; Gapinski, J.; Butt, H.-J. et al. Comparative analysis of viscosity of complex liquids and cytoplasm of mammalian cells at the nanoscale. *Nano Lett.* **2011**, *11*, 2157–2163.
- (34) Pan, A. C.; Borhani, D. W.; Dror, R. O.; Shaw, D. E. Molecular determinants of drug–receptor binding kinetics. *Drug discovery today* **2013**, *18*, 667–673.
- (35) Bordello, J.; Novo, M.; Al-Soufi, W. Exchange-dynamics of a neutral hydrophobic dye in micellar solutions studied by fluorescence correlation spectroscopy. *J. Colloid Interface Sci.* **2010**, *345*, 369–376.
- (36) Reuss, M.; Engelhardt, J.; Hell, S. W. Birefringent device converts a standard scanning microscope into a STED microscope that also maps molecular orientation. *Opt. Express* **2010**, *18*, 1049–1058.
- (37) Schönau, T.; Siebert, T.; Härtel, R.; Eckhardt, T.; Klemme, D.; Lauritsen, K.; Erd-

- mann, R. Pulsed picosecond 766 nm laser source operating between 1-80 MHz with automatic pump power management. *Proc. SPIE* **2013**, *8604*, 860409.
- (38) Vicidomini, G.; Moneron, G.; Han, K. Y.; Westphal, V.; Ta, H.; Reuss, M.; Engelhardt, J.; Eggeling, C.; Hell, S. W. Sharper low-power STED nanoscopy by time gating. *Nat. Methods* **2011**, *8*, 571–573.
- (39) Moffitt, J. R.; Osseforth, C.; Michaelis, J. Time-gating improves the spatial resolution of STED microscopy. *Opt. Express* **2011**, *19*, 4242–4254.
- (40) Dertinger, T.; Rüttinger, S. *Advanced Photon Counting: Applications, Methods, Instrumentation*; Springer, 2015.
- (41) Koenig, M.; Reisch, P.; Dowler, R.; Kraemer, B.; Tannert, S.; Patting, M.; Clausen, M. P.; Galiani, S.; Eggeling, C.; Koberling, F. et al. Ns-time resolution for multispecies STED-FLIM and artifact free STED-FCS. *Proc. SPIE* **2016**, *9712*, 97120T.